



Fast and robust numerical solutions to minimal problems for cameras with radial distortion

Zuzana Kukelova^{a,*}, Martin Byröd^b, Klas Josephson^b, Tomas Pajdla^a, Kalle Åström^b

^aCenter for Machine Perception, Dept. of Cybernetics, Faculty of Elec. Eng., Czech Technical University Prague, 12135 Prague, Czech Republic

^bCentre for Mathematical Sciences, Lund University, Lund, Sweden

ARTICLE INFO

Article history:

Received 18 March 2008

Accepted 21 November 2008

Available online 24 December 2008

Keywords:

Radial distortion calibration

Minimal problems

Gröbner Basis

ABSTRACT

A number of minimal problems of structure from motion for cameras with radial distortion have recently been studied and solved in some cases. These problems are known to be numerically very challenging and in several cases there were no practical algorithms yielding solutions in floating point arithmetic. We make some crucial observations concerning the floating point implementation of Gröbner basis computations and use these new insights to formulate fast and stable algorithms for two minimal problems with radial distortion previously solved in exact rational arithmetic only: (i) simultaneous estimation of essential matrix and a common radial distortion parameter for two partially calibrated views and six image point correspondences and (ii) estimation of fundamental matrix and two different radial distortion parameters for two uncalibrated views and nine image point correspondences. We demonstrate that these two problems can be efficiently solved in floating point arithmetic in simulated and real experiments. For comparison we have also invented a new non-minimal algorithm for estimating fundamental matrix and two different radial distortion parameters for two uncalibrated views and twelve image point correspondences based on a generalized eigenvalue problem.

© 2008 Elsevier Inc. All rights reserved.

1. Introduction

Estimating camera motion and internal calibration parameters from sequences of images is a challenging computer vision problem with a broad range of applications [1]. One typically starts with a noisy set of tentative image point correspondences. The first step then is to make decisions about correct and incorrect matches and get a good initial estimate to be able to deploy a more sophisticated optimization algorithm on the set of all correct matches.

Two robust and widely used techniques for this purpose are RANSAC [2] and kernel voting [3], both relying on solving a large number of instances of the underlying problem, each with a small number of point correspondences. There is thus a need to develop fast and stable algorithms for solving geometric vision problems with a minimal number of points. This typically amounts to solving a system of polynomial equations in several variables. These problems are known to be numerically very challenging and in several cases there exist no practical algorithms yielding solutions in floating point arithmetic.

Traditionally, minimal problems have been formulated assuming a linear pin-hole camera model with different restrictions on the internal calibration parameters. However, for some cameras such as fish-eye lenses, this can be insufficient and

one might need to handle strong radial distortions already from the outset.

The particularly interesting solution to the simultaneous estimation of the fundamental matrix and single radial distortion parameter, based on the division model, has been introduced by Fitzgibbon [4]. His formulation leads to solving a system of algebraic equations. Fitzgibbon, however, did not use all the algebraic constraints on the fundamental matrix. Thanks to neglecting some of the constraints, he could work with a very special system of algebraic equations that can be solved numerically by using a quadratic eigenvalue solver (QEP). Micusik and Pajdla [5,6] also neglected the constraints when formulating the estimation of a paracatadioptric camera model from image matches as a quartic eigenvalue problem.

Li and Hartley [7] treated the original Fitzgibbon's problem as a system of algebraic equations and used the hidden variable technique [8] to solve them. Their technique thus solves exactly the same problem as [4] but in a different way.

Solving for the fundamental matrix under different radial distortions was first studied in [9], where a *non-minimal* algorithm based on 15 point correspondences was given for a pair of uncalibrated cameras.

More recently [10,11], a number of different *minimal* problems with radial distortion have been studied and practical solutions were given in some cases.

* Corresponding author.

E-mail address: kukelova@cmp.felk.cvut.cz (Z. Kukelova).

The state-of-the-art method for solving polynomial equations is based on calculations with Gröbner bases [12] and has many applications in computer vision, but also in other fields such as cryptography [13] and robotics [14]. In [15,16] Gröbner bases were used to derive a fast algorithm for globally optimal three view triangulation under the L_2 -norm.

In this paper we further develop the techniques of numerical Gröbner basis computations. In particular, we (i) note the importance of obtaining a single elimination step in the Gröbner basis computation, (ii) give guidelines how this can be achieved and (iii) we present a new simplified formulation of the Gröbner basis computation procedure based on LU factorization, which reduces the computational burden of the elimination step.

Leveraging on these new insights, we formulate fast and numerically stable algorithms for two minimal problems with radial distortion previously unsolved in floating point arithmetic: (i) simultaneous estimation of essential matrix and a common radial distortion parameter for two partially calibrated views and six image point correspondences and (ii) estimation of fundamental matrix and two different radial distortion parameters for two uncalibrated views and nine image point correspondences.

We demonstrate the speed and intrinsic numerical stability as well as robustness to noise of the proposed algorithms using both synthetic data and real images.

We compare our minimal algorithms with the existing Fitzgibbon's non-minimal algorithm [4] for estimating fundamental matrix \mathbf{F} and a single radial distortion from 9 point correspondences based on QEP, the Gröbner basis minimal algorithm [10] for a single radial distortion and 8 point correspondences, which uses $\det(\mathbf{F}) = 0$, a linear 16 point algorithm for estimating \mathbf{F} and two different radial distortions and finally with the new non-minimal algorithm for two different radial distortions based on the generalized eigenvalue problem proposed in this paper.

2. Review of Gröbner Basis techniques for polynomial equation solving

Solving systems of polynomial equations is a challenging problem in many respects and there exist no practical numerically stable algorithms for the general case. Instead, special purpose algorithms need to be developed for specific applications. The state-of-the-art tool for doing this is calculations with Gröbner bases [8].

Our general goal is to find the complete set of solutions to a system

$$f_1(\mathbf{x}) = 0, \dots, f_m(\mathbf{x}) = 0, \quad (1)$$

of m polynomial equations in n variables $\mathbf{x} = (x_1, \dots, x_n)$. The polynomials f_1, \dots, f_m generate an *ideal* I in $\mathbb{C}[\mathbf{x}]$, the ring of multivariate polynomials in \mathbf{x} over the field of complex numbers defined as the set

$$I = \{g(\mathbf{x}) : g(\mathbf{x}) = \sum_k h_k(\mathbf{x})f_k(\mathbf{x})\}, \quad (2)$$

where the $h_k(\mathbf{x})$ are any polynomials.

The Gröbner basis method for equation solving essentially builds on a generalization of polynomial division to the multivariate case. A concept arising in multivariate polynomial division which does not exist in the univariate case is division by a *set* of polynomials. See [8] for details. Division by an ideal as given by (2) can then be defined as division by the set of generators f_k .

The starting point now is to consider the space of all possible remainders under division by I . This space is denoted $\mathbb{C}[\mathbf{x}]/I$ and referred to as the *quotient space*. It can be seen as a generalization of the modulo rings \mathbb{Z}_n to polynomials. A famous result from algebraic

geometry now states that if the set of Eq. (1) has a finite set of zeros, then $\mathbb{C}[\mathbf{x}]/I$ will be a finite-dimensional linear space with dimension equal to the number of zeros of (1) [8].

With the space $\mathbb{C}[\mathbf{x}]/I$ in hand an elegant trick now yields the solutions to (1). Consider multiplication by one of the variables x_k . This generates a linear mapping from $\mathbb{C}[\mathbf{x}]/I$ to itself and since we are in a finite-dimensional space, by selecting an appropriate linear basis, this mapping can be represented as a matrix \mathbf{m}_{x_k} . This matrix is known as the *action matrix* and the eigenvalues of \mathbf{m}_{x_k} are exactly the values of x_k on the zeros of (1). Furthermore, the eigenvectors of $\mathbf{m}_{x_k}^T$ correspond to the vector of monomials evaluated at the zeros of (1) [8].

The crucial step in the process is to compute the remainder arithmetic of $\mathbb{C}[\mathbf{x}]/I$. Multivariate polynomial division by I is complicated by the fact that it is not well defined for most choices of generators. Consider the operator $\mathbf{P} : \mathbb{C}[\mathbf{x}] \rightarrow \mathbb{C}[\mathbf{x}]/I$ representing division by I for some choice of generators. For \mathbf{P} to be well defined we require that $\mathbf{P}(f_1(\mathbf{x}) + f_2(\mathbf{x})) = \mathbf{P}f_1(\mathbf{x}) + \mathbf{P}f_2(\mathbf{x})$ for all $f_1(\mathbf{x}), f_2(\mathbf{x}) \in \mathbb{C}[\mathbf{x}]$.

Fortunately there exist a canonical choice of generators for which \mathbf{P} is well defined. This set of generators of I is known as the Gröbner basis of I and allows direct construction of the action matrix [8]. Calculating the Gröbner basis of I is therefore our main concern. In general, this is accomplished by Buchberger's algorithm which works well in exact arithmetic. However, in floating point arithmetic it very easily becomes unstable. There exist some attempts to remedy this [17,18], but for more difficult cases the only reliable approach (so far) is to study a particular class of equations (e.g. relative orientation for calibrated cameras [19], optimal three view triangulation [15], etc.) and use knowledge of what the structure of the Gröbner basis should be to design a special purpose Gröbner basis solver. This method has been developed by Stewenius and others in a number of papers [12,10,20]. In the following section we outline how this is done and provide new insights enabling us to solve the two problems with radial distortion treated in this paper.

3. A matrix version of Buchberger's algorithm

The reason why Buchberger's algorithm breaks down in floating point arithmetic is that eliminations of monomials are performed successively and this causes round-off errors to accumulate to the point where it is completely impossible to tell whether a certain coefficient should be zero or not. The idea introduced by Faugere [17] is to write the list of equations in a matrix form

$$\mathbf{C} \begin{bmatrix} \mathbf{x}^{z_1} \\ \vdots \\ \mathbf{x}^{z_n} \end{bmatrix} = 0, \quad (3)$$

where $[\mathbf{x}^{z_1} \dots \mathbf{x}^{z_n}]^T$ is a vector of monomials with the notation $\mathbf{x}^{z_k} = x_1^{z_{k1}} \dots x_n^{z_{kn}}$. Elimination of leading terms now translates to matrix operations and we then have access to a whole battery of techniques from numerical linear algebra allowing us to perform many eliminations at the same time with control on pivoting etc.

However, as mentioned above, the real power of this approach is brought out by combining it with knowledge about a specific problem obtained in advance with a computer algebra system such as Macaulay2 [21]. One can then get information about exactly which monomials occur in Buchberger's algorithm and the dimension of $\mathbb{C}[\mathbf{x}]/I$.

3.1. Obtaining a single elimination step

With knowledge of the particular problem at hand, it is often ideal to obtain a single big elimination step. The reason for this is

that each elimination step can be ill conditioned and with errors accumulating the situation soon becomes hopeless. With a single elimination step we get maximal control over row pivoting etc. Moreover, the basis selection method introduced in [16] can further improve stability, but is only applicable when a single elimination step is possible.

In Buchberger's algorithm, two polynomials are picked and the least common multiple of their leading terms is eliminated by multiplying them with the right monomials and then subtracting them. This is done a large number of times until convergence. We mimic this process but aim at completely separating multiplication by monomials and elimination. The steps are

- (i) Multiply the original set of equations with a large number of monomials yielding an expanded set of equations.
- (ii) Stack the coefficients of these equations in an expanded coefficient matrix \mathbf{C}_{exp} .
- (iii) If enough new equations were generated in the previous step, row operations on \mathbf{C}_{exp} yield the elements of the Gröbner basis we need.

An important observation made independently in [16] and [10] is that not all elements of the Gröbner basis are needed. Let \mathcal{B} denote a selection of basis monomials for $\mathbb{C}[\mathbf{x}]/I$. Then to construct the action matrix \mathbf{m}_{x_k} we only need to calculate the elements of the ideal I with leading monomials in the set $(x_k \cdot \mathcal{B}) \setminus \mathcal{B}$.

Let \mathcal{M} denote the complete set of monomials and let $\mathcal{R} = (x_k \cdot \mathcal{B}) \setminus \mathcal{B}$ denote the set of monomials that need to be reduced to $\mathbb{C}[\mathbf{x}]/I$. Finally, let \mathcal{E} (\mathcal{E} for excessive) denote the remaining monomials. We then have a partitioning of the monomials as $\mathcal{M} = \mathcal{E} \cup \mathcal{R} \cup \mathcal{B}$.

Now, reorder the columns of \mathbf{C}_{exp} and the vector of monomials \mathbf{X} to reflect this

$$[\mathbf{C}_{\mathcal{E}} \quad \mathbf{C}_{\mathcal{R}} \quad \mathbf{C}_{\mathcal{B}}] \begin{bmatrix} \mathbf{X}_{\mathcal{E}} \\ \mathbf{X}_{\mathcal{R}} \\ \mathbf{X}_{\mathcal{B}} \end{bmatrix} = 0. \quad (4)$$

The \mathcal{E} -monomials are not in the basis and do not need to be reduced [16] so we eliminate them performing an LU factorization of \mathbf{C}_{exp} yielding the following schematic result:

$$\begin{bmatrix} \mathbf{U}_{\mathcal{E}1} & \mathbf{C}_{\mathcal{R}1} & \mathbf{C}_{\mathcal{B}1} \\ 0 & \mathbf{U}_{\mathcal{R}2} & \mathbf{C}_{\mathcal{B}2} \end{bmatrix} \begin{bmatrix} \mathbf{X}_{\mathcal{E}} \\ \mathbf{X}_{\mathcal{R}} \\ \mathbf{X}_{\mathcal{B}} \end{bmatrix} = 0, \quad (5)$$

where $\mathbf{U}_{\mathcal{E}1}$ and $\mathbf{U}_{\mathcal{R}2}$ are upper triangular. We can now discard the top rows of the coefficient matrix producing

$$[\mathbf{U}_{\mathcal{R}2} \quad \mathbf{C}_{\mathcal{B}2}] \begin{bmatrix} \mathbf{X}_{\mathcal{R}} \\ \mathbf{X}_{\mathcal{B}} \end{bmatrix} = 0. \quad (6)$$

From this we see that if the submatrix $\mathbf{U}_{\mathcal{R}2}$ is of full rank we get precisely the polynomials from the ideal I we need by forming

$$[\mathbf{I} \quad \mathbf{U}_{\mathcal{R}2}^{-1} \mathbf{C}_{\mathcal{B}2}] \begin{bmatrix} \mathbf{X}_{\mathcal{R}} \\ \mathbf{X}_{\mathcal{B}} \end{bmatrix} = 0, \quad (7)$$

or equivalently

$$\mathbf{X}_{\mathcal{R}} = -\mathbf{U}_{\mathcal{R}2}^{-1} \mathbf{C}_{\mathcal{B}2} \mathbf{X}_{\mathcal{B}}, \quad (8)$$

which means that the \mathcal{R} -monomials can now be expressed uniquely in terms of the \mathcal{B} -monomials. This is precisely what we need for computing the action matrix \mathbf{m}_{x_k} in $\mathbb{C}[\mathbf{x}]/I$. In other words, the property of $\mathbf{U}_{\mathcal{R}2}$ as being of full rank is sufficient to get the part of the remainder arithmetic of $\mathbb{C}[\mathbf{x}]/I$ that we need to compute \mathbf{m}_{x_k} .

4. Application to minimal problems with radial distortion

Based on the techniques described in the previous section, we are now able to provide fast and stable algorithms for two previously untractable minimal problems with radial distortion:

- (i) The problem of estimating a one-parameter radial distortion model and epipolar geometry from image point correspondences in two uncalibrated views with different radial distortions in each image.
- (ii) The problem of estimating a one-parameter radial distortion model and epipolar geometry from image point correspondences in two partially calibrated views.

These two problems were previously studied in [11] and found to be numerically very challenging. In [11], the authors provided solutions to these problems computed in exact rational arithmetic only. This results in very long computational times and is not usable in practical applications. In [22], an efficient way of getting the floating point solution has been suggested. This paper makes a synthesis of [11] and [22] and demonstrates that indeed the new solution is better than previous solutions in simulated and real experiments. Moreover this paper provides a new non-minimal solution to the problem of estimating fundamental matrix and two different radial distortion parameters for uncalibrated cameras and 12 point correspondences based on a generalized eigenvalue problem.

4.1. Uncalibrated case

In our solution we use the same formulation of the problem as in [11]. This formulation assumes a one-parameter division model [4] given by the formula

$$\mathbf{p}_u \sim \mathbf{p}_d / (1 + \lambda r_d^2) \quad (9)$$

where $\mathbf{p}_u = (x_u, y_u, 1)^T$ and $\mathbf{p}_d = (x_d, y_d, 1)^T$ are the corresponding undistorted, resp. distorted, image points, and r_d is the radius of \mathbf{p}_d w.r.t. the distortion center.

It is known that to get solutions to this minimal problem for uncalibrated cameras with different radial distortions λ_1 and λ_2 in each image, we have to use the epipolar constraint [1] for 9 point correspondences

$$\mathbf{p}_{u_i}^T(\lambda_1) \mathbf{F} \mathbf{p}_{u_i}'(\lambda_2) = 0, \quad i = 1, \dots, 9 \quad (10)$$

and the singularity of the fundamental matrix \mathbf{F}

$$\det(\mathbf{F}) = 0. \quad (11)$$

Assuming $f_{3,3} \neq 0$ we can set $f_{3,3} = 1$ and obtain 10 equations in 10 unknowns.

4.1.1. Eliminating variables

The epipolar constraint gives nine equations with 16 monomials $(f_{3,1}\lambda_1, f_{3,2}\lambda_1, f_{1,3}\lambda_2, f_{2,3}\lambda_2, \lambda_1\lambda_2, f_{1,1}, f_{1,2}, f_{1,3}, f_{2,1}, f_{2,2}, f_{2,3}, f_{3,1}, f_{3,2}, \lambda_1, \lambda_2, 1)$ and 10 variables $(f_{1,1}, f_{1,2}, f_{1,3}, f_{2,1}, f_{2,2}, f_{2,3}, f_{3,1}, f_{3,2}, \lambda_1, \lambda_2)$.

Among them, we have four variables which appear in one monomial only $(f_{1,1}, f_{1,2}, f_{2,1}, f_{2,2})$ and four variables which appear in two monomials $(f_{1,3}, f_{2,3}, f_{3,1}, f_{3,2})$. Since we have nine equations from the epipolar constraint we can use these equations to eliminate six variables, four variables which appear in one monomial only (and can be straightforwardly eliminated) and two of the variables which appear in two monomials. In this solution we have selected $f_{1,3}$ and $f_{2,3}$.

We reorder the monomials contained in the 9 equations and put the monomials containing $f_{1,1}, f_{1,2}, f_{2,1}, f_{2,2}, f_{1,3}$ and $f_{2,3}$ at the

beginning. The reordered monomial vector becomes $\mathbf{X} = [f_{1,1}, f_{1,2}, f_{2,1}, f_{2,2}, f_{1,3}, f_{2,3}, f_{3,1}, f_{3,2}, \lambda_1, \lambda_2, 1]^T$.

We rewrite the nine equations from the epipolar constraint on matrix form $\mathbf{C}\mathbf{X} = 0$, where \mathbf{C} is the coefficient matrix. After performing Gauss–Jordan (G–J) elimination on the matrix \mathbf{C} , we obtain nine equations on the form

$$f_i = LT(f_i) + g_i(f_{3,1}, f_{3,2}, \lambda_1, \lambda_2) = 0, \quad (12)$$

where $LT(f_i) = f_{1,1}, f_{1,2}, f_{2,1}, f_{2,2}, f_{1,3}, f_{2,3}, f_{3,1}, f_{3,2}$ resp. $f_{3,1}, \lambda_1$ for $i = 1, 2, 3, 4, 5, 6, 7, 8$ resp. 9 and $g_i(f_{3,1}, f_{3,2}, \lambda_1, \lambda_2)$ are 2nd order polynomials in four variables $f_{3,1}, f_{3,2}, \lambda_1, \lambda_2$. This means that we can express the 6 variables, $f_{1,1}, f_{1,2}, f_{1,3}, f_{2,1}, f_{2,2}, f_{2,3}$ as functions of the other four variables $f_{3,1}, f_{3,2}, \lambda_1, \lambda_2$.

$$\begin{aligned} f_{1,1} &= -g_1(f_{3,1}, f_{3,2}, \lambda_1, \lambda_2) \\ f_{1,2} &= -g_2(f_{3,1}, f_{3,2}, \lambda_1, \lambda_2) \\ f_{1,3} &= -g_6(f_{3,1}, f_{3,2}, \lambda_1, \lambda_2) \\ f_{2,1} &= -g_3(f_{3,1}, f_{3,2}, \lambda_1, \lambda_2) \\ f_{2,2} &= -g_4(f_{3,1}, f_{3,2}, \lambda_1, \lambda_2) \\ f_{2,3} &= -g_8(f_{3,1}, f_{3,2}, \lambda_1, \lambda_2), \end{aligned} \quad (13)$$

Substituting these expressions into the other three equations from the epipolar constraint and also into the singularity constraint for \mathbf{F} gives four polynomial equations in four unknowns (one of 2nd degree, two of 3rd degree and one of 5th degree)

$$\begin{aligned} \lambda_2(-g_6(f_{3,1}, f_{3,2}, \lambda_1, \lambda_2)) + g_5(f_{3,1}, f_{3,2}, \lambda_1, \lambda_2) &= 0 \\ \lambda_2(-g_8(f_{3,1}, f_{3,2}, \lambda_1, \lambda_2)) + g_7(f_{3,1}, f_{3,2}, \lambda_1, \lambda_2) &= 0 \\ f_{3,1}\lambda_1 + g_9(f_{3,1}, f_{3,2}, \lambda_1, \lambda_2) &= 0 \\ \det \begin{pmatrix} -g_1 & -g_2 & -g_6 \\ -g_3 & -g_4 & -g_8 \\ f_{3,1} & f_{3,2} & 1 \end{pmatrix} &= 0. \end{aligned} \quad (14)$$

This problem has 24 solutions in general [11].

4.1.2. The Solver

The numerical solver is constructed starting with the four remaining Eq. (14) in the four unknowns $f_{3,1}, f_{3,2}, \lambda_1$ and λ_2 . The first step is to expand the number of equations, as outlined in Section 3, by multiplying them by a handcrafted set of monomials in the four unknowns yielding 393 equations in 390 monomials. See Section 4.1.3 for details.

The coefficients of the equations are then stacked in a matrix \mathbf{C} as in (3). Following this, the monomials are ordered as in (4). The sets \mathcal{E} and \mathcal{R} depend on which variable is used to create the action matrix. For this problem $f_{3,1}$ was used as the “action” variable. The classical method is thereafter to choose the linear basis \mathcal{B} of $\mathbb{C}[\mathbf{x}]/I$ to be the 24 lowest monomials (*w.r.t.* some monomial order). This is enough to get a solution to the problem, but as mentioned in Section 3 we can use the method introduced in [16] to select a basis of linear combinations of monomials from a larger set and thereby improve numerical stability. Empirically, we have found that the linear basis can be selected from the set of all monomials up to degree four excluding the monomial λ_1^4 . The set \mathcal{R} then consists of monomials of degree five that are reached when the monomials of degree four are multiplied with $f_{3,1}$. \mathcal{E} is the remaining set of 285 monomials.

Putting the part of \mathbf{C} corresponding to \mathcal{E} and \mathcal{R} on triangular form by means of an LU decomposition now produces (5). We can then remove all equations that include excessive monomials and still have enough information to construct the action matrix.

Finally, we make the choice of representatives for $\mathbb{C}[\mathbf{x}]/I$ by the method in [16] and do the last elimination to get the part of the Gröbner basis we need to construct the action matrix.

4.1.3. Details on the expansion step for the uncalibrated case

We have found experimentally that to construct the necessary elements of the Gröbner basis, we need to generate polynomials up to a total degree of eight. Thus, the 2nd degree polynomial has to be multiplied with all monomials up to degree six and monomials with the corresponding degrees for the 3rd and 5th degree polynomials.

Further investigations has shown that not exactly all monomials up to degree eight are needed, so in the implementation the 2nd degree polynomial was only multiplied with monomials up to degree five and each variable not higher than four. Moreover λ_1 was not multiplied with degrees higher than two. For the other polynomials it was possible to limit the degree of each individual variable to one lower than the total degree.

These multiplications yield 393 equations in 390 monomials. Without the last fine tuning of the degrees, the number of equations and monomials will be larger but all extra monomials will be in the set \mathcal{E} and will make no real difference to the solver except slightly longer computation times.

4.2. Calibrated case

To solve the minimal problem for calibrated cameras, we make use of the epipolar constraint for 6 point correspondences

$$\mathbf{p}_{u_i}^\top(\lambda) \mathbf{E} \mathbf{p}_{u_i}'(\lambda) = 0, \quad i = 1, \dots, 6, \quad (15)$$

the singularity of the essential matrix \mathbf{E}

$$\det(\mathbf{E}) = 0 \quad (16)$$

and the trace constraint, which says that two singular values of the essential matrix are equal

$$2(\mathbf{E}\mathbf{E}^\top)\mathbf{E} - \text{trace}(\mathbf{E}\mathbf{E}^\top)\mathbf{E} = 0. \quad (17)$$

Again assuming $e_{3,3} \neq 0$, we can set $e_{3,3} = 1$ and obtain 16 equations in 9 unknowns.

4.2.1. Eliminating variables

The epipolar constraint gives 6 equations in 15 monomials ($\lambda e_{1,3}, \lambda e_{2,3}, \lambda e_{3,1}, \lambda e_{3,2}, \lambda^2, e_{1,1}, e_{1,2}, e_{1,3}, e_{2,1}, e_{2,2}, e_{2,3}, e_{3,1}, e_{3,2}, \lambda, 1$) and 9 variables ($e_{1,1}, e_{1,2}, e_{1,3}, e_{2,1}, e_{2,2}, e_{2,3}, e_{3,1}, e_{3,2}, \lambda$).

Using a similar elimination method as in the uncalibrated case we eliminate 5 of these 9 variables. All these variables can be eliminated simultaneously.

We have again four variables which appear in one monomial only ($e_{1,1}, e_{1,2}, e_{2,1}, e_{2,2}$) and four variables which appear in two monomials ($e_{1,3}, e_{2,3}, e_{3,1}, e_{3,2}$). Since we have six equations of which each contains all 15 monomials we can eliminate five of these nine variables. We select the first four variables $e_{1,1}, e_{1,2}, e_{2,1}, e_{2,2}$ that appear in one monomial only and the fifth variable as $e_{1,3}$ which appears in two monomials.

We reorder the monomials contained in the 6 equations putting monomials containing $e_{1,1}, e_{1,2}, e_{2,1}, e_{2,2}$ and $e_{1,3}$ at the beginning. The reordered monomial vector will be $\mathbf{X} = [e_{1,1}, e_{1,2}, e_{2,1}, e_{2,2}, e_{1,3}, \lambda, e_{1,3}, e_{2,3}, e_{3,1}, e_{3,2}, \lambda^2, e_{2,3}, e_{3,1}, e_{3,2}, \lambda, 1]^T$.

We rewrite 6 equations from the epipolar constraint on matrix form $\mathbf{C}\mathbf{X} = 0$. After performing G–J elimination on the matrix \mathbf{C} , we obtain 6 equations of the form

$$f_i = LT(f_i) + g_i(e_{2,3}, e_{3,1}, e_{3,2}, \lambda) = 0, \quad (18)$$

where $LT(f_i) = e_{1,1}, e_{1,2}, e_{2,1}, e_{2,2}, e_{1,3}, \lambda$, resp. $e_{1,3}$ for $i = 1, 2, 3, 4, 5$ resp. 6 and $g_i(e_{2,3}, e_{3,1}, e_{3,2}, \lambda)$ are 2nd order polynomials in four variables $e_{2,3}, e_{3,1}, e_{3,2}, \lambda$.

So, the five variables $e_{1,1}, e_{1,2}, e_{1,3}, e_{2,1}, e_{2,2}$ can be expressed as functions of the other four variables $e_{2,3}, e_{3,1}, e_{3,2}, \lambda$.

$$\begin{aligned}
e_{1,1} &= -g_1(e_{2,3}, e_{3,1}, e_{3,2}, \lambda) \\
e_{1,2} &= -g_2(e_{2,3}, e_{3,1}, e_{3,2}, \lambda) \\
e_{1,3} &= -g_6(e_{2,3}, e_{3,1}, e_{3,2}, \lambda) \\
e_{2,1} &= -g_3(e_{2,3}, e_{3,1}, e_{3,2}, \lambda) \\
e_{2,2} &= -g_4(e_{2,3}, e_{3,1}, e_{3,2}, \lambda).
\end{aligned} \tag{19}$$

We substitute these expressions into the remaining equation from the epipolar constraint and into the singularity and trace constraints for \mathbf{E} . In this way we obtain 11 polynomial equations in 4 unknowns (one of degree 3, four of degree 5 and six of degree 6):

$$\lambda(-g_6(e_{2,3}, e_{3,1}, e_{3,2}, \lambda)) + g_5(e_{2,3}, e_{3,1}, e_{3,2}, \lambda) = 0, \tag{20}$$

$$\text{one equation from the singularity constraint} \\ \det(\mathbf{E}) = 0, \tag{21}$$

$$\text{and 9 equations from the trace constraint} \\ 2(\mathbf{E}\mathbf{E}^T)\mathbf{E} - \text{trace}(\mathbf{E}\mathbf{E}^T)\mathbf{E} = 0, \tag{22}$$

with

$$\mathbf{E} = \begin{pmatrix} -g_1 & -g_2 & -g_6 \\ -g_3 & -g_4 & e_{2,3} \\ e_{3,1} & e_{3,2} & 1 \end{pmatrix}. \tag{23}$$

In [11] it was shown that this problem has 52 solutions.

4.2.2. The solver

The numerical solution of this problem largely follows that of the uncalibrated version. In the first expansion, all equations are multiplied with monomials to reach degree eight. This gives 356 equations in 378 monomials. As in the uncalibrated case it is possible to reduce the number of monomials by fine tuning the degrees we need to use, in this case yielding 320 equations in 363 monomials.

The next step is to reorder the monomials as in Eq. (4). Once again, the linear basis of $\mathbb{C}[\mathbf{x}]/I$ can be constructed from the mono-

nomials of degree four and lower. \mathcal{B} will then consist of those monomials of degree five that are reached when the degree four monomials are multiplied with the variable $e_{3,1}$, which is used as the “action” variable.

As before, \mathbf{C} is transformed to triangular form by LU decomposition and after that we only consider those equations that do not include any of the monomials in \mathcal{E} . Now \mathbf{C} holds all necessary information to choose representatives in $\mathbb{C}[\mathbf{x}]/I$ by the method of [16] and create the action matrix with respect to multiplication by $e_{3,1}$.

5. Non-minimal solution to the uncalibrated case with different distortions

For comparison we have also created a new non-minimal algorithm for estimating fundamental matrix and two different radial distortion parameters for two uncalibrated views and twelve image point correspondences based on the generalized eigenvalue problem. This algorithm is similar to the well-known algorithm for estimating \mathbf{F} and a single distortion parameter from nine point correspondences proposed by Fitzgibbon [4] which was formulated as a quadratic eigenvalue problem.

We also formulate the problem with different distortions as a generalized eigenvalue problem. We use equations from the epipolar constraint for 12 point correspondences

$$\mathbf{p}_{u_i}^T(\lambda_1)\mathbf{F}\mathbf{p}_{u_i}'(\lambda_2) = 0, \quad i = 1, \dots, 12. \tag{24}$$

Assuming $f_{3,3} \neq 0$ we can set $f_{3,3} = 1$ and obtain 12 equations with 16 monomials

$(f_{3,1}\lambda_1, f_{3,2}\lambda_1, f_{1,3}\lambda_2, f_{2,3}\lambda_2, \lambda_1\lambda_2, f_{1,1}, f_{1,2}, f_{1,3}, f_{2,1}, f_{2,2}, f_{2,3}, f_{3,1}, f_{3,2}, \lambda_1, \lambda_2, 1)$

and 10 variables $(f_{1,1}, f_{1,2}, f_{1,3}, f_{2,1}, f_{2,2}, f_{2,3}, f_{3,1}, f_{3,2}, \lambda_1, \lambda_2)$.

Using the standard notation for the division model

$$\mathbf{p}_u(\lambda) \sim (x_d, y_d, 1 + \lambda r_d^2)^T, \tag{25}$$

we can rewrite the equations from the epipolar constraint as

$$(D_1 + \lambda_2 D_2)\mathbf{v} = \mathbf{0}, \tag{26}$$

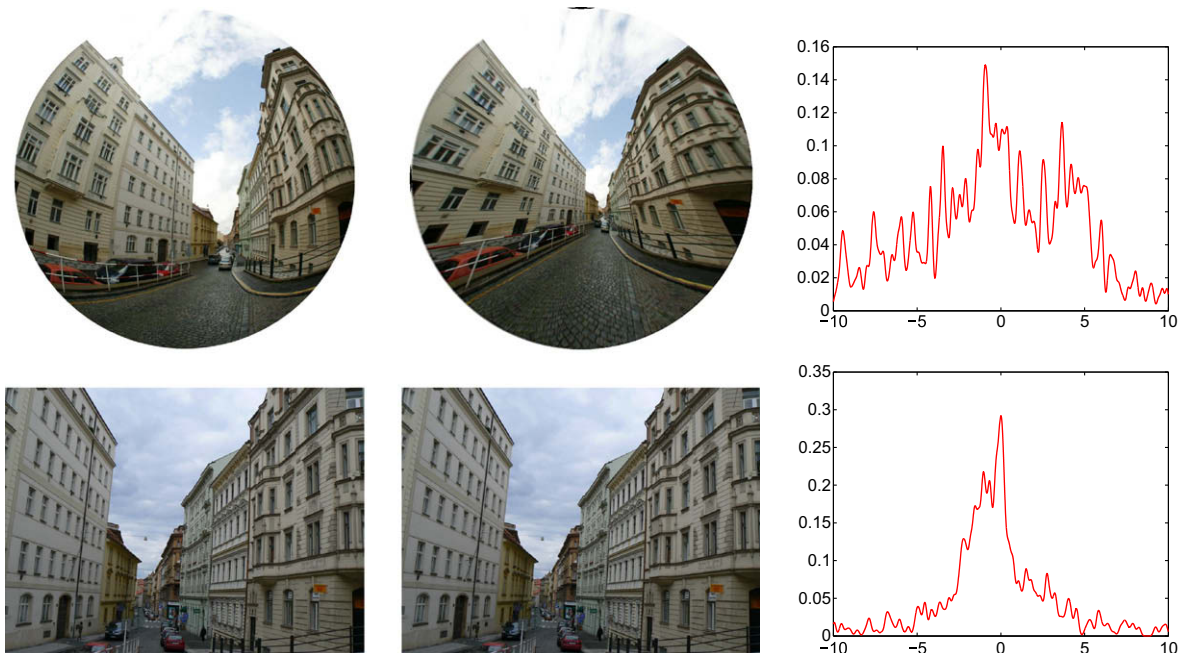


Fig. 1. (Left) Input images with different radial distortions (Top) 66% cutout (120° FOV) from a 180° FOV omnidirectional image and (Bottom) image taken with a standard perspective camera with very mild distortion. (Center) Corrected images. (Right) Distribution of real roots obtained by kernel voting. Estimated $\lambda_1 = -0.925625$ and $\lambda_2 = 0.002500$.

where $D_1 \equiv [x_d, x'_d, x_d, y'_d, x_d, y_d, x'_d, y'_d, x'_d, y_d, x_d, y_d, r^2_d, x'_d, r^2_d, y'_d, r^2_d, 1]$ and $D_2 \equiv [0, 0, x_d, r^2_d, 0, 0, y_d, r^2_d, 0, 0, 0, 0, r^2_d, r^2_d, r^2_d, i, 1, \dots, 12]$, $i = 1, \dots, 12$, are 12×12 matrices containing only known distorted coordinates and \mathbf{v} is the 12×1 vector of unknown monomials $\mathbf{v} = [f_{11}, f_{12}, f_{13}, f_{21}, f_{22}, f_{23}, f_{31}, f_{32}, f_{3,1}\lambda_1, f_{3,2}\lambda_1, \lambda_1, 1]$. The formulation (26) is a generalized eigenvalue problem which can be easily solved using standard efficient algorithms. For example MATLAB provides the function `polyeig`.

Because D3 has eight zero columns, this generalized eigenvalue problem leads to eight “infinite” eigenvalues. Thus, there are at most four finite real solutions to this problem.

6. Experiments

We have tested the algorithms for the uncalibrated and calibrated minimal problems on synthetic images with various levels of noise, outliers and radial distortions as well as on real images (Fig. 1). For comparison we have also tested our new non-minimal algorithm on synthetic images. The time of computation has been measured for both minimal algorithms. The minimal algorithms proposed in this paper are significantly more stable than the algorithms presented in [11] which ran in exact rational arithmetic only. Since doing the computations in exact arithmetic is extre-

mely slow (minutes instead of milliseconds), a comparison with the floating point algorithm presented in this paper is not meaningful and has therefore been omitted.

The problems presented in this paper are solved by finding the roots of a system of polynomial equations which means that we obtain several potentially correct answers, 52 in the calibrated case, 24 in the uncalibrated minimal case and 4 in the uncalibrated non-minimal case. In general we obtain more than one real root (Fig. 2), in which case we need to select the best one, *i.e.* the root which is consistent with most measurements. To do so, we treat the real roots obtained by solving the equations for one input as real roots from different inputs and use kernel voting [3] for several inputs to select the best root among all generated roots. The kernel voting is done using a Gaussian kernel with fixed variance and the estimates of λ_1 and λ_2 in the uncalibrated case and λ in the calibrated case are found as the positions of the largest peaks [3,10].

6.1. Tests on synthetic images

For all problems treated in this paper, the same synthetic experiments were carried out to evaluate the quality of the solvers.

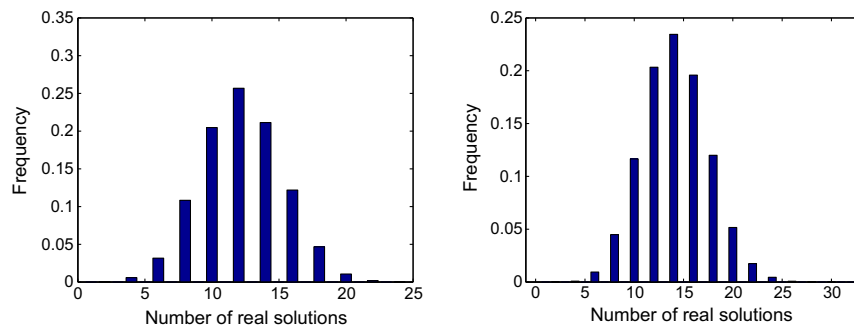


Fig. 2. (Left) The number of real solutions for the uncalibrated case. (Right) The number of real solutions for the calibrated case.

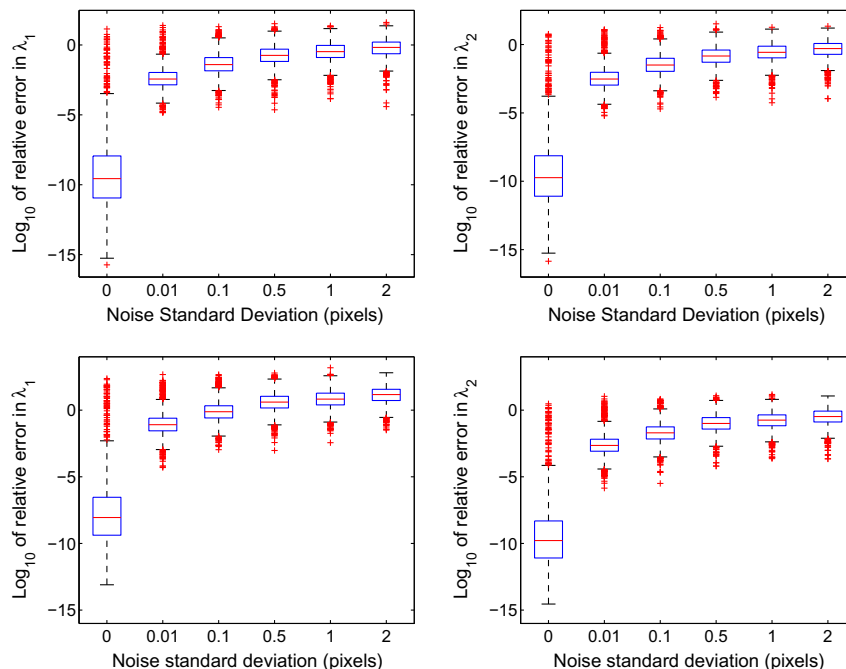


Fig. 3. Uncalibrated case: relative errors of (Left) λ_1 and (Right) λ_2 as a function of noise. Ground truth (Top) $\lambda_1 = -0.2, \lambda_2 = -0.3$ and (Bottom) $\lambda_1 = -0.01, \lambda_2 = -0.7$. Blue boxes contain values from 25% to 75% quantile. (For interpretation of the references to colour in this figure legend, the reader is referred to the web version of this paper.)

In all our simulated experiments we generate our synthetic data using the following procedure:

- (i) Generate a 3D scene consisting of 1000 points distributed randomly within a cube. Project $M\%$ of the points on image planes of the two displaced cameras, these are matches. In both image planes, generate $(100 - M)\%$ random points distributed uniformly in the image, these are mismatches. Altogether, they become undistorted correspondences, true as well as false matches.
- (ii) Apply different radial distortions to the undistorted correspondences in each image and in this way generate noiseless distorted points.
- (iii) Add Gaussian noise of standard deviation σ to the distorted points.

6.1.1. Uncalibrated case

In the first two experiments we study the robustness of our minimal as well as non-minimal algorithm for the uncalibrated case to Gaussian noise added to the distorted points.

The first experiment investigates the estimation error of λ as a function of noise. Results for the minimal algorithm are presented in Fig. 3 and for the non-minimal algorithm in the Fig. 4. The ground truth radial distortions parameters were $\lambda_1 = -0.2$, $\lambda_2 = -0.3$ Figs. 3 and 4 (Top) in the first case and $\lambda_1 = -0.01$, $\lambda_2 = -0.7$ Figs. 3 and 4 (Bottom) in the second case. The noise varied from 0 to 2 pixels. For each noise level relative errors for 2000 λ 's (estimated as the closest values to the ground truth value from all solutions) were computed. The results in Figs. 3 and 4 for the estimated $\bar{\lambda}_1$ (Left) and $\bar{\lambda}_2$ (Right) are presented by the Matlab function *boxplot* which shows values of the 25% to 75% quantiles as a blue box with red horizontal line at median. The red crosses show data beyond 1.5 times the interquartile range.

Both algorithms give similar results. For noiseless data we obtain very accurate estimates of radial distortion parameters even for very different λ 's. For larger noises the \log_{10} relative errors are much higher (mostly around 10^{-1}). However obtained

λ 's are still satisfactory and mostly differ from the ground truth value in the second decimal place. The main point though is not to use a one set of points to get a good estimate, but to repeatedly draw configurations from a larger set of potential matches and then use e.g. kernel voting to get a more reliable estimate. Finally, the result can be further enhanced using the obtained estimate as a good starting guess in a large scale bundle adjustment. The effect of kernel voting is studied in the second experiment.

In this experiment we did not select the root closest to the ground truth value for each run of the algorithm, instead we used kernel voting to select the best λ 's among all generated roots from several runs. The ground truth radial distortion parameters were as in the previous experiment ($\lambda_1 = -0.2$, $\lambda_2 = -0.3$ in the first case and $\lambda_1 = -0.01$, $\lambda_2 = -0.7$ in the second case) and the level of noise varied from 0 to 2 pixels. Moreover, in the first case there were 10% of mismatches in the image ($M=90$).

The testing procedure was as follows:

- (i) Repeat K times (We use K from 50 to 100 though for more noisy data K from 100 to 200 gives better results).
 - (a) Randomly choose 9 point correspondences from a set of N potential correspondences (6 point correspondences for the calibrated case).
 - (b) Normalize image point coordinates to $[-1, 1]$.
 - (c) Find 24 roots using our algorithm (4 roots for the non-minimal algorithm and 52 for the calibrated case).
 - (d) Select the real roots in the feasible interval, i.e. $-1 < \lambda_1$, $\lambda_2 < 1$ and the corresponding \mathbf{F} 's.
- (ii) Use kernel voting to select the best root.

Fig. 5 shows λ 's computed using our minimal algorithm for the uncalibrated case as a function of noise and Fig. 6 shows λ 's computed using our non-minimal algorithm. In the first case with mismatches Figs. 5 and 6 (Top) 100 λ 's were estimated using kernel voting for roots computed from 100 ($K = 100$) 9-tuples of correspondences randomly drawn for each noise level. In the second

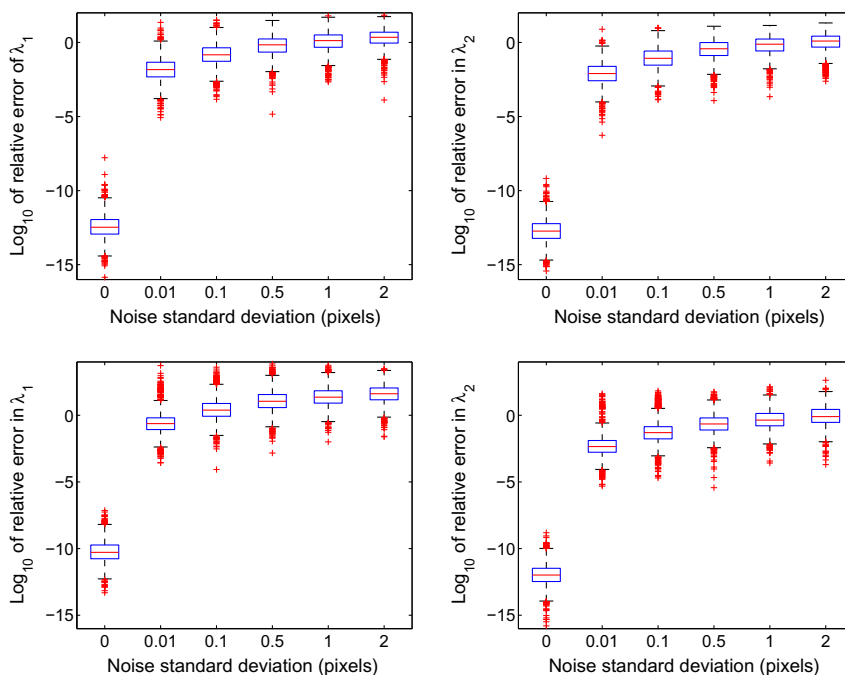


Fig. 4. Non-minimal “12 point” algorithm for uncalibrated case: relative errors of (Left) $\bar{\lambda}_1$ and (Right) $\bar{\lambda}_2$ as a function of noise. Ground truth (Top) $\lambda_1 = -0.2$, $\lambda_2 = -0.3$ and (Bottom) $\lambda_1 = -0.01$, $\lambda_2 = -0.7$. Blue boxes contain values from 25% to 75% quantile. (For interpretation of the references to colour in this figure legend, the reader is referred to the web version of this paper.)

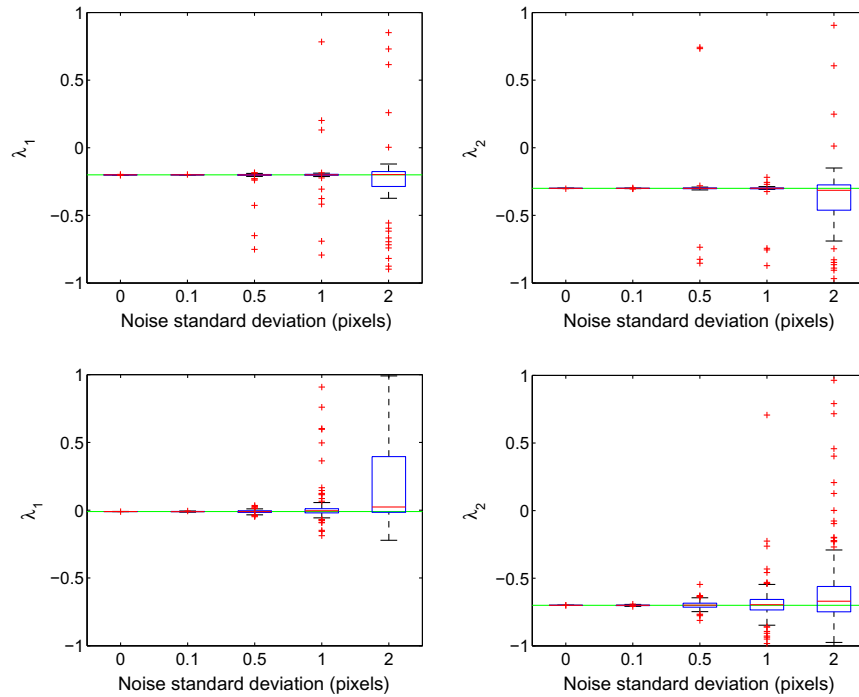


Fig. 5. Uncalibrated case, kernel voting: estimated (Left) $\bar{\lambda}_1$ and (Right) $\bar{\lambda}_2$ as a function of noise, (Top) ground truth $\lambda_1 = -0.2$, $\lambda_2 = -0.3$ (green lines), 90% of inliers and 100 samples in kernel voting and (Bottom) ground truth $\lambda_1 = -0.01$, $\lambda_2 = -0.7$, 100% of inliers and 50 samples in kernel voting. (For interpretation of the references to colour in this figure legend, the reader is referred to the web version of this paper.)

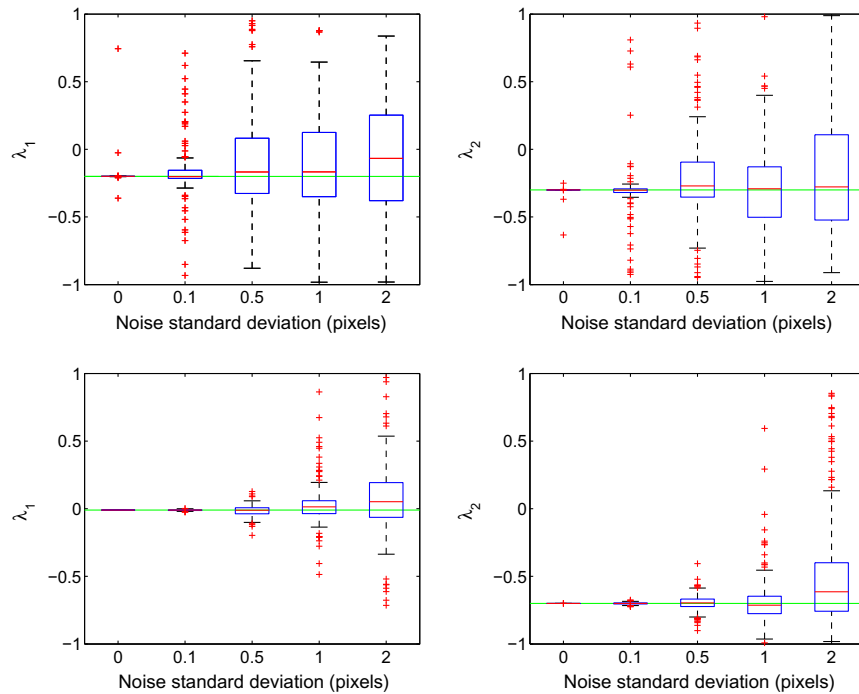


Fig. 6. Non-minimal “12 point” algorithm for uncalibrated case, kernel voting: estimated (Left) $\bar{\lambda}_1$ and (Right) $\bar{\lambda}_2$ as a function of noise, (Top) ground truth $\lambda_1 = -0.2$, $\lambda_2 = -0.3$ (green lines), 90% of inliers and 100 samples in kernel voting and (Bottom) ground truth $\lambda_1 = -0.01$, $\lambda_2 = -0.7$, 100% of inliers and 50 samples in kernel voting. (For interpretation of the references to colour in this figure legend, the reader is referred to the web version of this paper.)

case Figs. 5 and 6 (Bottom) 200 λ 's were estimated using kernel voting for roots computed from 50 ($K = 50$) 9-tuples of correspondences. This means that for each noise level our algorithm ran 10,000 times in both cases.

The results are again presented by the Matlab function *boxplot*.

For the minimal algorithm the median values for $\bar{\lambda}_1$ and $\bar{\lambda}_2$ are very close to the ground truth value for all noise levels from 0 to

2 pixels and also for very different radial distortion parameters Fig. 5 (Bottom) and 10% of mismatches Fig. 5 (Top).

The median values for the non-minimal “12 point” algorithm are also close to the ground truth values for all noise levels and also for very different radial distortion parameters Fig. 6 (Bottom) and 10% of mismatches Fig. 6 (Top). However, the variances of this “12 point” algorithm are considerably larger, especially for higher

noise levels, than the variances of the minimal algorithm Fig. 5. It is significant especially for data with mismatches Fig. 6 (Top). This is because for 12 points we have higher probability of choosing contaminated sample (sample containing mismatches) than for 9 points. The minimal algorithm thus produces higher number of good estimates for the fixed number of samples. This is good both for RANSAC as well as for kernel voting.

6.1.2. Calibrated case

The same synthetic experiments were carried out for the calibrated solver.

The results of the first experiment which shows relative errors of the estimated $\bar{\lambda}$ as a function of noise are shown in Fig. 7. The ground truth radial distortion was $\lambda = -0.3$. For noiseless data we again obtain very precise estimates of radial distortion parameter λ . For larger noise levels the \log_{10} relative errors are slightly larger than for the uncalibrated case. However, using kernel voting we can still obtain good estimates. This is shown by our second experiment.

In this experiment λ was estimated 50 times using kernel voting for roots computed from 200 6-tuples of correspondences randomly drawn for each noise level, Fig. 7. The median values for $\bar{\lambda}$ are again very close to the ground truth value $\lambda = -0.3$ for all noise levels from 0 to 2 pixels. However the variances of this for the calibrated case are larger, especially for higher noise levels, than the variances for the uncalibrated case. This means that for good estimates of λ this algorithm requires more samples in the kernel voting procedure than in the uncalibrated case.

6.1.3. RANSAC experiment

In the last experiment we compare our algorithms with other existing algorithms within the RANSAC paradigm by showing the number of correct matches recovered as a function of the number of samples made from a set of tentative matches contaminated by

mismatches. The number of samples used for our experiment was 10, 100 and 1000. We compare the following algorithms

- (i) Fitzgibbon's non-minimal algorithm [4] for estimating fundamental matrix \mathbf{F} and single radial distortion from nine point correspondences based on QEP;
- (ii) Gröbner based minimal algorithm [10] for estimating \mathbf{F} and single radial distortion from eight point correspondences, which uses $\det(\mathbf{F}) = 0$;
- (iii) Our new minimal algorithm for estimating \mathbf{E} and single radial distortion for calibrated cameras from 6 point correspondences, which uses constraints $\det(\mathbf{E}) = 0$ and $2\mathbf{E}\mathbf{E}^T\mathbf{E} - \text{trace}(\mathbf{E}\mathbf{E}^T)\mathbf{E} = 0$;
- (iv) Linear algorithm for estimating \mathbf{F} and two different radial distortions from 16 point correspondences;
- (v) Our new non-minimal algorithm for estimating \mathbf{F} and two different radial distortions from 12 point correspondences based on the generalized eigenvalue problem;
- (vi) Our new minimal algorithm for estimating \mathbf{F} and two different radial distortions from nine point correspondences, which uses $\det(\mathbf{F}) = 0$.

Two sets of images I1, I2 were generated using the procedure described in Subsection 6.1, I1 for $\lambda_1 = \lambda_2$ and I2 for $\lambda_1 \neq \lambda_2$. Gaussian noise with standard deviation 1 pixel was added to the image coordinates.

The number of correct matches ($M\%$ of correct matches) among 1000 tentative matches was fixed and the image points were corrupted by $(100 - M)\%$ of random mismatches. In our case M varies from 100% to 80%.

Table 1 shows results of the first 3 algorithms (i-iii) for single radial distortion $\lambda = -0.3$ and fixed threshold $\tau = 1$ pixel on the distance of an image point to epipolar curves. The results were obtained as a mean values from 100 runs of RANSAC for 10, 100 and

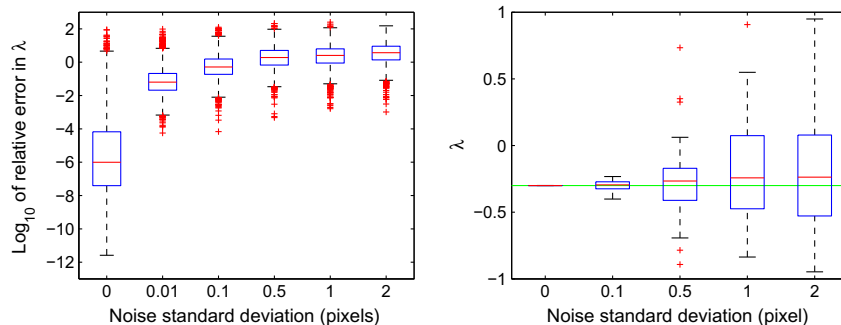


Fig. 7. Calibrated case: (Left) relative errors of $\bar{\lambda}$ as a function of noise, ground truth $\lambda = -0.3$. (Right) kernel voting: Estimated $\bar{\lambda}$ using kernel voting for roots computed from 200 6-tuples of correspondences randomly drawn for each noise level. Ground truth $\lambda = -0.3$ (green line). (For interpretation of the references to colour in this figure legend, the reader is referred to the web version of this paper.)

Table 1
The comparison of our “single distortion” algorithm for calibrated cameras with other existing algorithms within the RANSAC paradigm by showing the number of matches $K1$ within τ threshold and the number of correct matches $K2$ among them as a function of the number of samples made from a set of tentative matches contaminated by mismatches. The number of samples was 10, 100 and 1000, noise level was 1 pixel and threshold $\tau = 1$ pixel. Number of mismatches varied from 0–20%.

RANSAC experiment for $\lambda_1 = \lambda_2$										
Algorithm		No mismatches			10% Mismatches			20% Mismatches		
		10	100	1000	10	100	1000	10	100	1000
Fitzgibbon 9pt	K1	631.44	826.75	873.35	479.17	671.42	772.4	302.17	532.04	632.1
	K2	631.44	826.75	873.35	479.08	671.332	772.36	301.5	531.9	632.06
Kukelova 9pt	K1	695.62	835.38	835.38	520.84	685.67	773.36	322.36	574.65	660.5
	K2	695.62	835.38	835.38	520.73	685.6	773.28	321.78	574.54	660.36
Our minimal 6pt	K1	787.5	898.55	930.88	662.24	780.85	838.94	517.98	675.49	719.2
	K2	787.5	898.55	930.88	662.07	780.6	838.78	517.53	675.22	718.96

1000 samples. Table 2 shows results of the last 3 algorithms (iv-vi) for different radial distortions $\lambda_1 = -0.2$ and $\lambda_2 = -0.3$ and fixed threshold $\tau = 1$ pixel. The first row in both tables shows the number of matches $K1$ within τ threshold and the second row shows the number of correct matches $K2$ among them.

The results show that the algorithms sampling fewer points faster hit a non-contaminated sample than the algorithms sampling more points. Therefore, our minimal algorithms give better results than non-minimal algorithms. This is significant especially for higher number of mismatches.

6.2. Time consumption

To evaluate the speed of the new algorithm a reasonably optimized version of the algorithm for the uncalibrated case was implemented. The implementation was done in Matlab so rewriting the algorithm in a compiled language such as C should reduce the execution time further.

The algorithm was run 10,000 times and the time consumption was measured using the Matlab profiler. The experiments were performed on an Intel Core 2 CPU 2.13 GHz machine with 2 GB of memory. The estimated average execution time for solving one instance of the uncalibrated problem was 16 ms. The corresponding time for the calibrated problem was 17 ms. The time consuming parts of the algorithms are the initial LU-factorization and the eigenvalue decomposition and these are of comparable sizes.

These results are to be compared with the execution times given for the same problem in [11], where solutions were computed in exact rational arithmetic. There, the processing time for one problem instance was 30 s for the uncalibrated case and 1700 s for the calibrated case.

6.3. Tests on real images

We have tested our minimal algorithm for uncalibrated cameras with different radial distortions on several different sets of images. In the first experiment the input images with different relatively large distortions in each image, Fig. 8 (Left), were obtained as 60% cutouts from fish-eye images taken with two different cameras with different radial distortions. Tentative point matches were then found by the wide base-line matching algorithm [23]. They contained correct as well as incorrect matches. Distortion parameters λ_1 and λ_2 were estimated using our algorithm for uncalibrated cameras with different radial distortions and the kernel voting method for 100 samples. The input (Left) and corrected (Center) images are presented in Fig. 8. Fig. 8 (Right) shows the distribution of real roots for these images, from which $\lambda_1 = -0.301250$ and $\lambda_2 = -0.368125$ were estimated as the argument of the maximum. The peaks from kernel voting are sharp and the λ 's are estimated accurately.

In the second experiment we tested our algorithm on images with significantly different distortions. The left image Fig. 1

Table 2

The comparison of our minimal “different distortion” algorithm and our non-minimal “different distortion” algorithm with the linear 16 point algorithm within the RANSAC paradigm by showing the number of matches $K1$ within τ threshold and the number of correct matches $K2$ among them as a function of the number of samples made from a set of tentative matches contaminated by mismatches. The number of samples was 10, 100 and 1000, noise level was 1 pixel and threshold $\tau = 1$ pixel. Number of mismatches varied from 0–20%.

RANSAC experiment for $\lambda_1 \neq \lambda_2$										
Algorithm		No mismatches			10% Mismatches			20% Mismatches		
		10	100	1000	10	100	1000	10	100	1000
Linear 16pt	K1	316.34	681.22	748.03	232.55	415.7	485.1	86.48	322.35	328.06
	K2	316.34	681.22	748.03	232.55	415.69	485.08	86.459	322.31	328.04
Our non-minimal 12pt	K1	418.18	697.93	763.51	242.4	546.27	546.27	148.55	414.5	528.02
	K2	418.18	697.93	763.51	242.33	546.22	575.56	148.51	414.44	527.85
Our minimal 9pt	K1	625.03	801.98	845.76	513.03	671.77	732.56	342.23	538.85	654.86
	K2	625.03	801.98	845.76	512.71	671.67	732.54	341.31	538.4	654.65

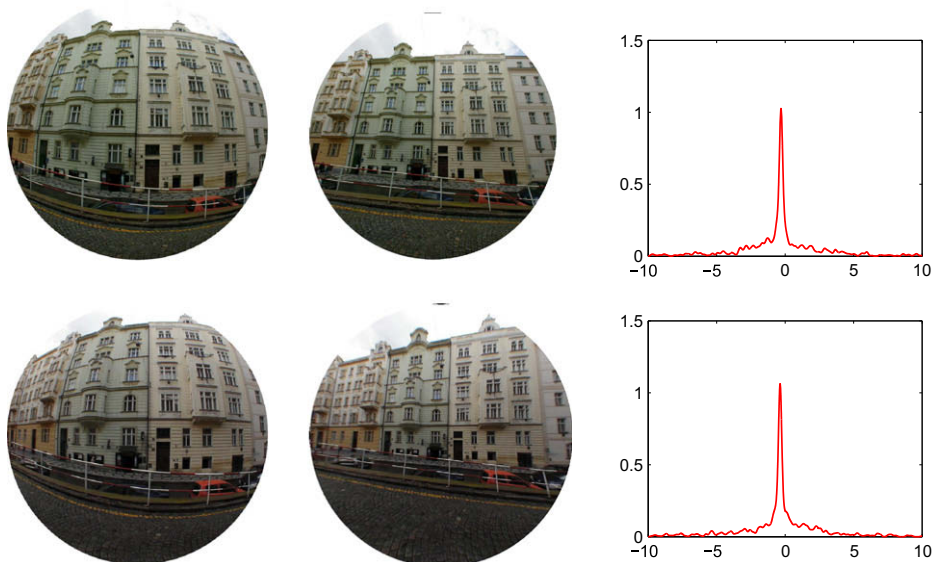


Fig. 8. Real data, 60% cutouts from omnidirectional images. (Left) Input images with different radial distortions for camera 1 (Top) and camera 2 (Bottom). (Center) Corrected images. (Right) Distribution of real roots obtained by kernel voting. Estimated $\lambda_1 = -0.301250$ and $\lambda_2 = -0.368125$.

(Top), was obtained as a 66% cutout (120° FOV) from a 180° FOV fish-eye image and the right image Fig. 1 (Bottom) was taken with a standard perspective camera. Since these images had a rather large difference in radial distortion, the tentative point correspondences contained a larger number of mismatches. Distortion parameters λ_1 and λ_2 were again estimated using our algorithm for uncalibrated cameras with different radial distortions and the kernel voting method. The input (Left) and corrected (Center) images are presented in Fig. 1. Fig. 1 (Right) shows the distribution of real roots for these images from which $\lambda_1 = -0.925625$ and $\lambda_2 = 0.002500$ were estimated. As can be seen the peaks obtained by kernel voting are not so sharp but still sufficient to get good estimates of the λ 's even from only 100 samples.

7. Conclusions

In this paper we have given fast and robust algorithms for two minimal problems for simultaneous computation of epipolar geometry and radial distortion in floating point arithmetic. The two problems of simultaneously solving for relative pose and radial distortion were, due to numerical problems, previously solved in exact rational arithmetic only, making them too time consuming to be of practical value. With the floating point algorithm presented in this paper we have reduced the computation time from minutes to milliseconds. Moreover, we have verified that this is done without loss of numerical precision by extensive experiments both on synthetic and real images.

We have also proposed a non-minimal algorithm for estimating \mathbf{F} and two different radial distortions from 12 point correspondences based on a generalized eigenvalue formulation.

In the experiments we have demonstrated that the radial distortion estimation is robust both to outliers and noise when kernel voting is used over several runs. Finally, we have shown that large differences in distortion between two images can be handled.

Acknowledgements

This work has been supported by Grants EU FP7-SPA-218814 PRiVisG and MSM6840770038 DMCM III and the Swedish Research Council through Grant No. 2005-3230 Geometry of multi-camera systems, Grant No. 2004-4579 Image- Based Localisation and Recognition of Scenes.

References

[1] R.I. Hartley, A. Zisserman, in: *Multiple View Geometry in Computer Vision*, second ed., Cambridge University Press, 2004, ISBN 0521540518.

- [2] M.A. Fischler, R.C. Bolles, Random sample consensus: a paradigm for model fitting with applications to image analysis and automated cartography, *Communications of the ACM* 24 (6) (1981) 381–395.
- [3] H. Li, R. Hartley, A non-iterative method for lens distortion correction from point matches, in: *Workshop on Omnidirectional Vision*, Beijing China, 2005.
- [4] A.W. Fitzgibbon, Simultaneous linear estimation of multiple view geometry and lens distortion, in: *Proceedings of Computer Vision and Pattern Recognition Conference (CVPR)*, 2001, pp. 125–132.
- [5] B. Micusik, T. Pajdla, Estimation of omnidirectional camera model from epipolar geometry (2003) 485–490.
- [6] B. Micusik, T. Pajdla, Structure from motion with wide circular field of view cameras, *IEEE Transactions on Pattern Analysis and Machine Intelligence* 28 (7) (2006) 1135–1149.
- [7] H. Li, R. Hartley, A non-iterative method for correcting lens distortion from nine-point correspondences, in: *Proceedings of OmniVision05, ICCV-workshop*, 2005.
- [8] D. Cox, J. Little, D. O'Shea, *Ideals, Varieties, and Algorithms*, Springer-Verlag, 2007.
- [9] J. Barreto, K. Daniilidis, Fundamental matrix for cameras with radial distortion, in: *IEEE International Conference on Computer Vision*, Beijing, China, 2005.
- [10] Z. Kukulova, T. Pajdla, A minimal solution to the autocalibration of radial distortion, in: *Proceedings of Computer Vision and Pattern Recognition Conference (CVPR)*, IEEE Press, 2007.
- [11] Z. Kukulova, T. Pajdla, Two minimal problems for cameras with radial distortion, in: *Proceedings of The Seventh Workshop on Omnidirectional Vision, Camera Networks and Non-classical Cameras (OMNIVIS)*, 2007.
- [12] H. Stewénius, Gröbner basis methods for minimal problems in computer vision, Ph.D. thesis, Lund University, 2005.
- [13] J.-C. Faugère, A. Joux, Algebraic cryptanalysis of hidden field equation (hfe) cryptosystems using gröbner bases, in: *CRYPTO*, 2003, pp. 44–60.
- [14] A. Almadi, A. Dhingra, D. Kohli, A gröbner-sylvester hybrid method for closed-form displacement analysis of mechanisms, *Journal of Mechanical Design* 122 (4) (2000) 431–438.
- [15] H. Stewénius, F. Schaffalitzky, D. Nistér, How hard is three-view triangulation really? in: *Proc. 10th Int. Conf. on Computer Vision*, Beijing, China, 2005, pp. 686–693.
- [16] M. Byröd, K. Josephson, K. Åström, Improving numerical accuracy of gröbner basis polynomial equation solver, in: *International Conference on Computer Vision*, 2007.
- [17] J.-C. Faugère, A new efficient algorithm for computing grobner bases (f4), *Journal of Pure and Applied Algebra* 139 (1999) 61–88.
- [18] J.-C. Faugère, A new efficient algorithm for computing gröbner bases without reduction to zero (f5), in: *Proceedings of the 2002 international Symposium on Symbolic and Algebraic Computation*, ACM Press, New York, NY, USA, 2002, pp. 75–83.
- [19] H. Stewénius, C. Engels, D. Nistér, Recent developments on direct relative orientation, *ISPRS Journal of Photogrammetry and Remote Sensing* 60 (2006) 284–294.
- [20] H. Stewénius, D. Nistér, M. Oskarsson, K. Åström, Solutions to minimal generalized relative pose problems, in: *Workshop on Omnidirectional Vision*, Beijing China, 2005.
- [21] D. Grayson, M. Stillman, *Macaulay 2*, 1993–2002. Available from: <http://www.math.uiuc.edu/Macaulay2/>, an open source computer algebra software. <http://www.math.uiuc.edu/Macaulay2/>.
- [22] M. Byröd, Z. Kukulova, K. Josephson, T. Pajdla, K. Åström, Fast and robust numerical solutions to minimal problems for cameras with radial distortion, in: *Proc. Conference on Computer Vision and Pattern Recognition*, Anchorage, Alaska, USA, 2008.
- [23] J. Matas, O. Chum, M. Urban, T. Pajdla, Robust wide-baseline stereo from maximally stable extremal regions, *Image Vision Computing* 22 (10) (2004) 761–767.